2019 International Conference on Robotics and Automation (ICRA)
Palais des congres de Montreal, Montreal, Canada, May 20-24, 2019

Modeling Variable Curvature Parallel Continuum Robots Using Euler Curves

Phanideep S. Gonthina[1], Apoorva D. Kapadia[1], Isuru S. Godage[2] and Ian. D. Walker[1]

Abstract— **In this paper, we propose and investigate a new approach to modeling variable curvature continuum robot sections, based on Euler spirals. Euler spirals, also termed Clothoids, or Cornu spirals, are those curves in which the curvature increases linearly with their arc length. In this work, Euler spirals are applied to the kinematic modeling of continuum robots for the first time. The approach was evaluated using the sections of numerous continuum robots, including two novel parallel continuum robots. Each robot consists of three parallel sections, each with three thin, long McKibben actuators. These sections are poorly modeled by the widely used constant curvature kinematic model. The constant curvature and Euler spiral models were compared and the Euler spiral method was seen to be a significantly better match for a wide range of configurations of the robot hardware.**

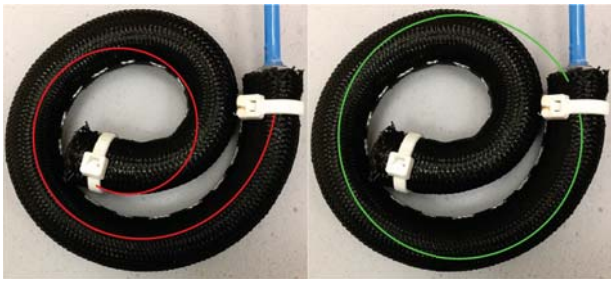

Fig. 1: Euler (in red) vs constant curvature (in green) modeling on a section developed in [27]

.

I. Introduction

Continuum robots, which are currently the subject of much research, have a continuous backbone structure. Unlike traditional rigid-link robots which are largely inspired by human (vertebrate) limbs, they lack rigid links and joints (like the elbow). An elephant trunk or a snake is more representative of the form of a continuum robot. These robots are usually inspired by nature and many robots which mimic continuum structures seen in nature have been built in recent years. Some of the work inspired by animals includes that by elephant trunks [1], [2], [3], octopus arms [4], [5], [6] snakes [7], and tails [8], [9]. Continuum robots have also been inspired by plants as seen in [10], [11].

Continuum and soft robotics have been the subject of rapid developments in the past few years, expanding their capabilities in medicine [12], [13], space [14], inspection [11], [15], [16] and other applications [17]. High precision and accuracy are expected from robots, especially in the medical field and commercial industry. To achieve this, accurate kinematic and dynamic models for continuum robots are essential. Various kinematics and dynamics modeling approaches have been applied to continuum robots. The constant curvature model [18] is by far the most widely used kinematic model. This model assumes that the continuum structure can be approximated as a serially connected set of constant curvature sections.

Chirikjian [19] introduced a general method for modeling continuum kinematics and dynamics. His approach uses modal functions to represent the curve shaping function. However, it has restrictions on the class of shapes it is able to approximate, due to the modal functions selected. Problems such as singularity in constant curvature models were addressed in [20] and a solution via an alternative modal model approach was presented. Another noteworthy model by Mochiyama [21] uses the Serret-Frenet formulae to develop the kinematics. These approaches support constant or variable curvature functions. A comparative study of five kinematic modeling methods - lumped system dynamic model [22], constant curvature [18], two-step modified constant curvature [23], variable curvature kinematics [24] with Cosserat rod and beam theory [25], and series solution identification - is detailed in [26]. The prevailing choice in continuum robot modeling remains constant curvature.

However, no continuum section has precisely constant curvature, and some exhibit highly variable curvature. The work in [28] proposes a model for a wire driven continuum manipulator with variable curvature. While this and other variable curvature modeling approaches, as in [24], [29], [30], have been shown to better approximate the shape of some continuum robot sections, they are generally computationally complex and non-intuitive, relative to constant curvature modeling. This paper introduces a new, computationally straightforward and intuitive approach to non-constant curvature modeling of continuum robot sections.

In the following section, we review the constant curvature approach. Section III introduces an alternative approach to variable curvature modeling, based on Euler spirals. The approach is evaluated on the sections of numerous continuum sections, including two novel parallel systems. These systems are introduced in Section IV, with results from the variable curvature modeling following in Section V. Section VI presents discussion and conclusions.

[1] P.S Gonthina, A.D. Kapadia, and I.D. Walker are with the Dept. of Electrical & Computer Engineering, Clemson University, Clemson, SC-29634-0915 ((pgonthi, akapadi, iwalker)@clemson.edu).
[2] I. S. Godage is with the School of Computing, DePaul University, Chicago, IL 60604 USA (e-mail: IGODAGE@depaul.edu).
This work was supported in part by the U.S. National Science Foundation under grants IIS-1527165 and IIS-1718075.

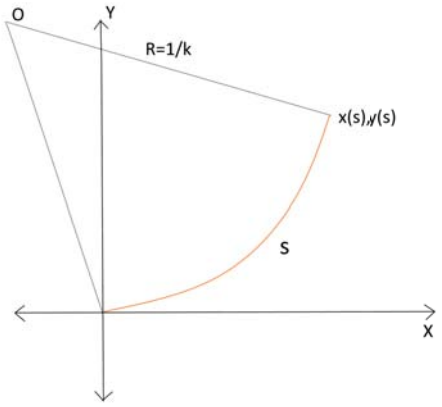

Fig. 2: Constant curvature kinematics

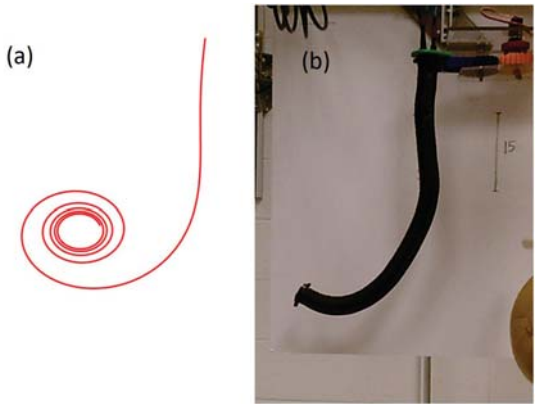

Fig. 3: (a) Euler curve - curvature increases linearly with arc length. (b) Example of a Mawby section curve

II. Constant Curvature Kinematic Modeling

Continuum robots are not well modeled using the same techniques that are used for rigid-link robots which use discrete joint angles exploiting constant link lengths of the robot. Arc lengths and curvatures better describe the shape of a continuum section. Due to the lack of an accurate model for the theoretically infinite degrees of freedom of a continuum structure, the constant curvature approximation has been widely used.

Various approaches have been used to formulate the constant curvature approximation, as discussed in [31]. For example, continuum kinematics via virtual rigid-link kinematics extends the Denavit-Hartenberg (D-H) convention, the standard approach for rigid-link robots, to solve for the tip position by generating the transformation matrix [32], [33]. The result (consistent with alternative, more geometrically direct approaches to constant curvature modeling) is summarized below.

For a planar continuum section as shown in Fig. 2 with the orange curved shape originating from the frame origin such that the initial tangent is aligned with the X-axis, the tip position equations are given by (1) and (2), where, $s \in \mathbb{R}^+$ is the arc length and $k \in \mathbb{R}^+$ is the curvature (given by $1/R$).

$$x = (1/k)(cos(sk) - 1) \tag{1}$$

$$y = (1/k)sin(sk) \tag{2}$$

where $(x \in \mathbb{R}, y \in \mathbb{R})$ is the tip position for given values of s and k.

III. Euler Spirals

The Euler spiral, also termed the Clothoid spiral, is a curve whose curvature is linearly proportional to its arc length (shown in Fig. 3). They are widely applied in railroads as transition curves (to transition from straight segments to circular curves). A clothoid approximation technique and its application in path planning application is detailed in [34]. Hirose's serpenoid curves are inspired by Clothoids [7].

Notice the visual resemblance of the early (proximal) part of the Euler spiral in Fig. 3(a), notably its steadily increasing curvature, to the curve exhibited in the continuum section in Fig. 3(b). In Section V, we will show that the curvatures of this section, and others forming part of the parallel continuum robot systems introduced in the following section, are closely modeled by Euler spirals. We believe that this strong shape match (which extends to other continuum sections of variable curvature), together with the inherent simplicity of the underlying formulation, suggests that Euler spirals warrant further consideration in continuum robot curvature modeling. Note the simple extension of the constant curvature model in the previous section to Euler spirals in (3) - (5) below allows them to inherit much of the convenience and low computational complexity of those models.

Recall that Euler spirals are defined to be those curves whose curvature increases linearly with arc length [35]. Given curvature $k \in \mathbb{R}^+$ and arc length $s \in \mathbb{R}^+$ this gives the equations below.

$$k = (1/r)s \tag{3}$$

where $r \in \mathbb{R}$ is a constant.

Substituting k by s/r in (1) and (2), Euler curve equations can be generated as follows:

$$x = (r/s)cos(s^2/r) \tag{4}$$

$$y = -(r/s)sin(s^2/r) \tag{5}$$

The values for x and y are undefined at $s = 0$, so in all numerical examples we start with $s = 0.01$.

The analytical form of the equations for Euler curves presents advantages compared to the synthetic curves studied in [30]. The explicit inclusion of the curvature provides a more direct way to visualize the curves than using the control points in synthetic curve approaches.

We next introduce two continuum robot systems with strongly variable curvature sections. These sections will be used to implement, validate, and explore the applicability of Euler curves to variable curvature modeling.

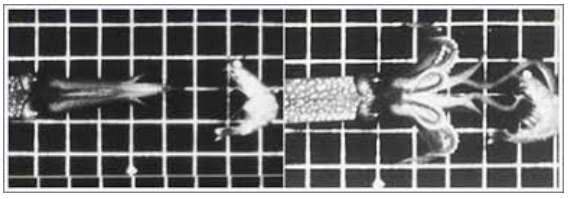

Fig. 4: Squid in prey capture. (Credit - William Kier, University of North Carolina, Chapel Hill)

IV. Two Novel Parallel Continuum Robots with Thin Sections

We introduce two continuum robot systems, named Separating Sections and Mawby. Each system features three degree of freedom sections operating in parallel.

Each section of the continuum robots discussed in this paper consists of three pneumatic McKibben actuators [36]. A key feature of both designs in the relatively long length of the sections, relative to their diameters. While the Separating Sections' sections have an average length of 45 cm and the muscles are connected by zip ties, Mawby's sections are about 56 cm each in length and connected with fishing line. To compare the size of these sections with those of an extensively studied serial continuum robot in our laboratory, the Octarm [37], the tip section of the Octarm has a length-diameter ratio of 6:1 whereas the ratio for the Mawby sections is close to 17:1 and that for Separating Sections is around 13.6:1. This higher length-diameter ratio for the Separating Sections and Mawby sections enables them to have a greater curl than the Octarm but this means they also demonstrate a considerably different curvature to the Octarm [37].

A. Separating Sections: A Squid-Inspired Robot

The underlying concept for the Separating Sections was to create a multi-purpose robot, which can operate as a single continuum robot with its three continuum "finger" sections aligned, but also have those fingers "open up" to form a parallel gripper. Motivation is provided by the way the squid deploys its arms and tentacles (see Fig. 4). The main design challenge was how to achieve the separation of the sections, which was done using fishing wire, as detailed below.

The design of Separating Sections is shown in Fig. 5(a). Zip ties were added to muscles 2,3,4,6,7 and 8 and fishing line was passed through these zip ties in a zig-zag fashion as shown in Fig. 5(b) to connect the three sections. The loose ends of the fishing line are terminated at the bottom and are fed back through the center of the 3 sections system and taken out from the top to be connected to servo motors. This was done to ensure the fishing line is loosened at the tip, where the sections branch out from, instead of the base.

When the fishing line is held taut, the sections work as a single unit. The system extends in length when all nine muscles are actuated. When a single section is actuated, the resulting motion mimics that of a three-muscle unit when a single muscle in that unit is actuated as shown in Fig. 5(c).

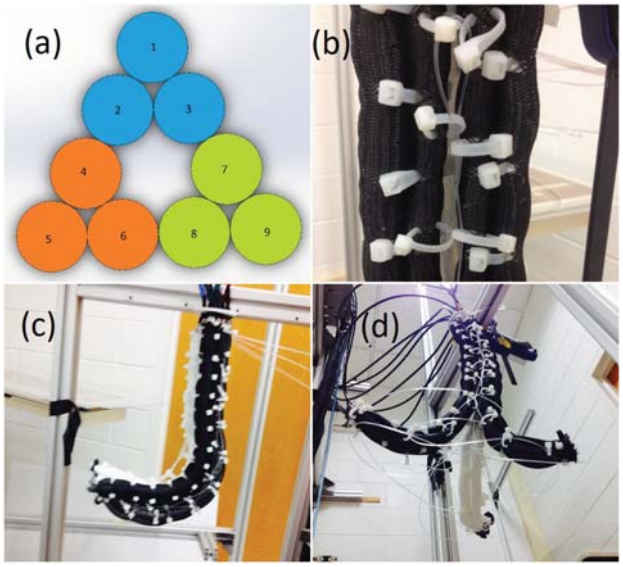

Fig. 5: (a) shows Separating Sections design. 3 sections comprising of 3 muscles each. Each color represents a different section. (b) The fishing line passing through the zip ties and connecting the muscles. (c) Separating Sections working as a single unit. (d) Separating Section working as three units.

When the fishing line was loosened, the three sections are not held together anymore and can branch out. Fig. 5(d) shows all three sections curving outwards. When the system is located directly above the object, the section can open up, hover around the object, and when in reach, the sections can close in and grasp objects.

B. Mawby: A Parallel Continuum Gripper

Mawby consists of three continuum sections in parallel, with a single degree of freedom rotation about their common base. In order to be able to grasp a wide range of objects, the design of this robot was inspired by the Barrett Hand [38]. In this design there are three robotic fingers. One finger is fixed while the other two can move 180° about the palm of the hand. The configurations to grasp objects can be made with a simple, single degree of freedom design. To construct a similar capability for Mawby, gears were printed using additive manufacturing. A servo motor was attached to the central gear and was able to move the two movable sections 180°. Two different orientations of the sections are shown in Fig. 6.

The robot designs introduced in this section represent a novel approach to continuum robot design. The Separating Sections is the first continuum robot that can operate as both an independent serial section and a parallel continuum robot. Mawby is the first parallel continuum robot in which the section base locations can be varied. Both feature high length to diameter ratio sections.

Experiments with prototype hardware realizations of the designs indicate that they can be highly effective in a variety

Fig. 6: Mawby in two different orientations. In the image on the left the two movable sections are 90° apart from the fixed section. In the image on the right the movable sections are 180° apart from the fixed section.

Fig. 7: Constant curvature modeling - Mawby

of novel adaptive grasping operations. One feature common to both robots is the uneven, non-constant, curvature of their sections. This is a function of their long, thin design, which proves effective in grasping. However, it makes their modeling a challenge. This issue is addressed, using Euler spirals, in the following section of the paper.

V. Use of Euler Curves

In order to analyze and predict the behavior of the continuum robots introduced in Section IV and continuum robots in general, variable curvature models are necessary. In this section, we apply Euler spirals to modeling the curvature of both long and short continuum sections and support the analysis with experimental validation.

To analyze the ability of both constant and non-constant curvature models to fit the continuum robots considered in Section IV, numerous images were captured from a fixed camera position of a Mawby section, first under various pressure values in which only one muscle was pressurized. For the range of $(0, s]$, using (1) and (2), constant curvature curves were subsequently matched to the shapes of the Mawby section shown in Fig. 7.

Due to the shape discrepancies clearly visible in the constant curvature images for Mawby sections there is a clear need for a better model. Using (4) and (5), Euler curves were generated to approximate the Mawby section curves. The input parameters for each curve in the example sets are seen in Table I and the corresponding results can be seen in Fig. 8. To calculate the error between the generated curve and Mawby section curve, 50 points were manually selected on the section image along the length of curve, starting from the base of the section and ending at the tip. The Euclidean distance between these points and the point closest to it in the generated Euler curve or constant curvature curve was calculated. The root-mean-square value of the error values for each point selected was calculated to achieve an error value for a given curve. The percentage error decrease is calculated by the formula in Equation 6.

Pressure (PSI)	r	s_1	s_2
13	0.092	0.014	0.56
16.25	0.072	0.14	0.57
19.5	0.044	0.16	0.6
22.75	0.042	0.19	0.62
26	0.04	0.2	0.635

TABLE I: Input values for Mawby - Euler spiral

$$\%\ error = (\frac{e1 - e2}{e1})100 \tag{6}$$

where e1 is the error from the constant curvature model and e2 is the error from the Euler model - both of which are shown in Table II.

Comparison of the Euler spiral model to the constant curvature model is seen in Table II. It can be seen visually in Fig.s 7 and 8, and numerically from Table II that the Euler spiral modeling is a significant improvement over the constant curvature modeling.

Pressure (PSI)	CC error e1 (in m)	Euler error e2 (in m)	Percent error decrease
13	0.0892	0.0061	93.16
16.25	0.05	0.0059	88.2
19.5	0.0443	0.0124	72.01
22.75	0.0388	0.0126	67.53
26	0.0389	0.0109	71.98

TABLE II: Error Comparison for Mawby - Euler spiral

Fig. 8: Euler modeling - Mawby (length of section: 56 cm)

Pressure (PSI)	r	s_1	s_2
13	0.084	0.016	0.51
16.25	0.075	0.16	0.525
19.5	0.066	0.155	0.53
26	0.059	0.155	0.535
29.25	0.047	0.145	0.52
32.5	0.042	0.14	0.52

TABLE III: Input values for Separating Sections - single muscle actuation

A. Separating Section - Single Muscle Actuation

The effect of this model was further investigated on the shorter sections of the Separating Sections robot discussed in Section IV. The Separating Sections' section curves were generated here by actuating a single muscle with the other two muscles unpressurized. The input parameters are as shown in Table III and their corresponding comparisons can be seen in Fig. 9. Comparison of the Euler spiral model to the constant curvature model is seen in Table IV.

B. Short Section - Single Muscle Actuation

A new 'short' section was constructed with length 25.4 cm and a length to diameter ratio of 7.7:1. This section exhibits curvature visually close to constant. The effect of the Euler model was further investigated on this short section. The input parameters are as shown in Table V and their corresponding comparisons can be seen in Fig. 10. Comparison of the Euler spiral model to the constant curvature model is seen in Table VI. It can be seen that even for "almost" constant curvature sections, the Euler curve method generates significantly better shape approximations.

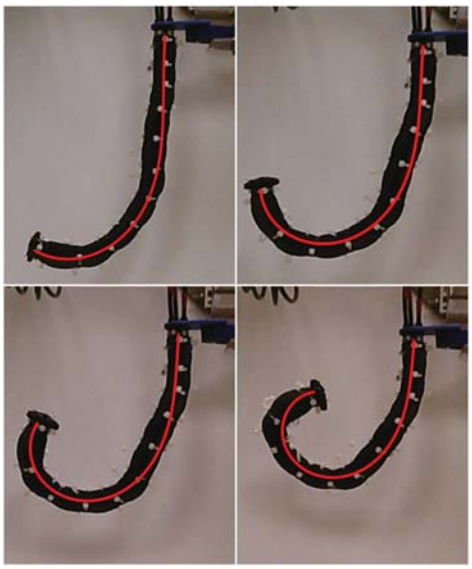

Fig. 9: Euler modeling - Separating Sections (length: 45 cm)

Pressure (PSI)	CC error e1 (in m)	Euler error e2 (in m)	Percent error decrease
13	0.0311	0.0043	86.17
16.25	0.0278	0.0057	79.5
19.5	0.0311	0.0069	72.01
26	0.0301	0.0065	78.41
29.25	0.0307	0.0075	71.98
32.5	0.0291	0.0063	78.35

TABLE IV: Error Comparison for Separating Sections - single muscle actuation

Pressure (PSI)	r	s_1	s_2
13	0.079	0.27	0.46
16.25	0.059	0.25	0.45
19.5	0.047	0.23	0.435
22.75	0.046	0.25	0.468
26	0.04	0.23	0.445
29.25	0.24	0.145	0.46
32.5	0.28	0.14	0.498

TABLE V: Input values for Short Section - single muscle actuation

Pressure (PSI)	CC error e1 (in m)	Euler error e2 (in m)	Percent error decrease
13	0.005	0.0027	46
16.25	0.0086	0.0022	74.42
19.5	0.0073	0.0023	68.49
22.75	0.0063	0.0026	55.56
26	0.0094	0.0024	74.47
29.25	0.0059	0.0033	44.07
32.5	0.0074	0.0032	56.76

TABLE VI: Error Comparison for Short Section - single muscle actuation

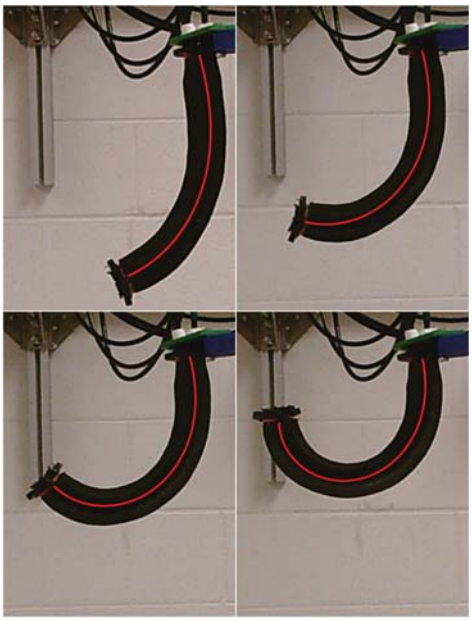

Fig. 10: Euler modeling - Short Section (length: 25.4 cm)

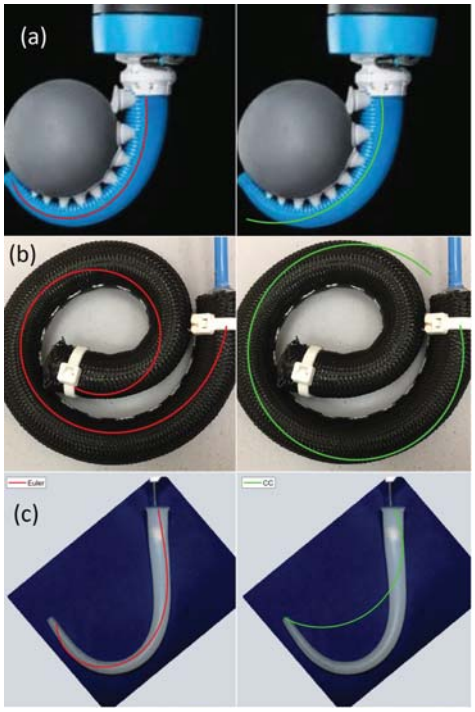

Fig. 11: Euler modeling - Other Robots. (a) OctopusGripper by Festo. Image taken from festo.com (accessed September 15, 2018). (b) Section developed in [27]. (c) Section developed in [39].

C. Other Continuum Robots

With the improvement of the Euler curves over the constant curvature model on the robots and sections designed in our laboratory, the effect of the Euler model was further investigated on curves generated by other soft/continuum robots designed outside our laboratory. Images were taken from references as noted or freely available on the internet. Fig. 11(a) shows the OctopusGripper designed by Festo. An 82% improvement in error was recorded by the Euler model compared to constant curvature model. Significant improvements were also recorded for sections developed in [27] (shown in 11(b)) and [39] (shown in 11(c)).

Numerous cases of the Mawby section and Separating Sections section curves were illustrated and analyzed in this paper. The effect of the Euler curve approach was investigated on 42 different curves generated by varying the pressures in the muscles of the robots discussed in Section IV [40]. It was found that the accuracy of the Euler curve approach is superior across a wide range of configurations.

VI. Conclusion and Future Work

This paper discussed the application of Euler spirals to the modeling of continuum robot sections exhibiting significant variable curvature. Euler spirals represent a straighforward extension from commonly used constant curvature models, with curvature increasing linearly as a function of length. Use of Euler spirals thus inherits many of the convenient properties of constant curvature approaches, and represents both an intuitive and a computationally simple approach to modeling variable curvature.

Euler spirals were used to model the curvature of two novel continuum manipulators introduced in this paper, Mawby and Separating sections. Mawby is a three section adaptive gripper, with its design inspired by the Barrett Hand, and is the first parallel continuum robot to feature adjustable relative section base positions. The three sections of Separating Sections can operate as a single serial section unit, but can also branch out into three separate and distinct units as the situation demands. A key enabling feature of both robots however, is the use of relatively long sections, which exhibit significant variability in their curvature.

Euler spirals were applied to 42 different curves generated by different combinations of pressure values in the three muscles of sections of Mawby and Separating Sections. When compared to the constant curvature model, the Euler spiral curves yielded a 93% improvement in predicting the shape in the sections of Mawby. The approach was applied to continuum sections of the Separating Sections robot and the results were also an improvement over the constant curvature model with an 86% decrease in error.

Euler spirals were also applied to a variety of other prominent continuum sections as well as one with close-to-constant curvature. The results again demonstrates the ability of Euler curves to significantly outperform constant curvature models.

For future work, we intend to work on the following:
1. Further develop the relationship between the input parameters and the shape parameters.
2. Comparison with other variable curvature techniques.
3. Extend analysis to multiple segments.

REFERENCES

[1] M. Hannan and I. Walker, "Analysis and experiments with an elephant's trunk robot," *Advanced Robotics*, vol. 15, no. 8, pp. 847–858, Aug. 2001.

[2] H. Tsukagoshi, A. Kitagawa, and M. Segawa, "Active hose: An artificial elephant's nose with maneuverability for rescue operation," in *Proc. IEEE Int. Conf. Robot. Autom.*, Seoul, Korea, 2001, pp. 2454–2459.

[3] A. Grzesiak, R. Becker, and A. Verl, "A bionic handling assistant - a success story of additive manufacturing," *Assembly Automation*, vol. 31, no. 4, pp. 329–333, Sep. 2011.

[4] W. McMahan, B. Jones, and I. Walker, "Robotic manipulators inspired by cephalopod limbs," *Jour. Eng. Des. Inno.*, vol. 1.

[5] E. Guglielmino, N. Tsagarakis, and D. Caldwell, "An octopus-anatomy inspired robotics arm," in *Proc. IEEE/RSJ Int. Conf. Intel. Robot. Syst.*, Taipei, 2010, pp. 3091–3096.

[6] M. Calisti, A. Arienti, F. Renda, G. Levi, B. Hochner, B. Mazzolai, P. Dario, and C. Laschi, "Design and development of a soft robot with crawling and gasping capabilities," in *Proc. IEEE Int. Conf. Robot. Autom.*, St. Paul, MN, 2012, pp. 4950–4955.

[7] S. Hirose, *Biologically Inspired Robots*. Oxford, UK: Oxford University Press, 1993.

[8] W. Rone and P. Ben-Tsvi, "Continuum robotic tail loading analysis for mobile robot stabilization and maneuvering," in *Proc. ASME Int. Design Engineering Technical Conferences & Computers and Information in Engineering Conference*, Buffalo, NY, 2014, pp. 1–8.

[9] J. L. C. Santiago, I. S. Godage, P. Gonthina, and I. D. Walker, "Soft robots and kangaroo tails: Modulating compliance in continuum structures through mechanical layer jamming," *Soft Robotics*, vol. 3, no. 2, pp. 54–63, Jun. 2016.

[10] Sadeghi, A. Tonazzini, I. Popova, and B. Mazzolai, "Robotic mechanism for soil penetration inspired by plant root," in *Proc. IEEE Int. Conf. Robot. Autom.*, Karlsruhe, Germany, 2013, pp. 3457–3462.

[11] M. Wooten, C. Frazelle, I. Walker, A. Kapadia, and J. Lee, "Exploration and inspection with vine-inspired continuum robots," in *Proc. IEEE Int. Conf. Robot. Autom.*, Brisbane, Australia, 2018, pp. 5526–5533.

[12] J. Burgner-Kars, D. Rucker, and H. Choset, "Continuum robots for medical applications: A survey," *IEEE Trans. Robot.*, vol. 31, no. 6, pp. 1261–1280, Dec. 2015.

[13] N. Simaan, R. Taylor, and P. Flint, "A dextrous system for laryngeal surgery," in *Proc. IEEE Int. Conf. Robot. Autom.*, New Orleans, LA, 2004, pp. 351–357.

[14] J. Mehling, M. Diftler, M. Chu, and M. Valvo, "A minimally invasive tendril robot for in-space inspection," in *Proc Biorobotics Conference*, Pisa, Italy, 2006, pp. 690–695.

[15] R. Buckingham, "Snake arm robots," *Ind. Robot: An Int. Jour.*, vol. 29, no. 3, pp. 242–245, Mar. 2002.

[16] X. Dong, D. Axinte, D. Palmer, S. Cobos, M. Raffles, A. Rabani, and J. Kell, "Development of a slender robotic system for on-wing inspection/repair of gas turbine engines," in *Robotics and Computer-Integrated Manufacturing*, 2017.

[17] H. Mao, J. Xiao, M. M. Zhang, and K. Daniilidis, "Shape-based object classication and recognition through continuum manipulation," in *Proc. IEEE/RSJ Int. Conf. Intel. Robot. Syst.*, Vancouver, BC, Canada, 2017, pp. 456–463.

[18] R. Webster III and B. A. Jones, "Design and modeling of constant curvature continuum robots," *Int. Jour. Robots. Res.*, vol. 29, no. 13, pp. 1661–1683, Jul. 2010.

[19] G. Chirikjian, "Hyper-redundant manipulator dynamics: A continuum approximation," *Adv. Robot.*, vol. 9, no. 3, pp. 217–243, Jun. 1995.

[20] I. Godage, E. Guglielmino, D. Branson, G. MedranoCerda, and D. Caldwell, "Novel modal approach for kinematics of multisection continuum arms," in *Proc. IEEE/RSJ Int. Conf. Intel. Robot. Syst.*, San Francisco, CA, 2011, pp. 1093–1098.

[21] H. Mochiyama and T. Suzuki, "Kinematics and dynamics of a cable-like hyper-flexible manipulator," in *Proc. IEEE Int. Conf. Robot. Autom.*, Taipei, Taiwan, 2003, pp. 3672–3677.

[22] I. S. Godage, R. Wirz, I. D. Walker, , and R. J. W. III, "Accurate and efficient dynamics for variable-length continuum arms: A center of gravity approach," *Soft Robotics*, vol. 2, no. 3, pp. 96–106, Jun. 2015.

[23] M. Mahvash and P. Dupont, "Stiffness control of a continuum manipulator in contact with a soft environment," in *Proc. IEEE/RSJ Int. Conf. Intel. Robot. Syst.*, Taipei, Taiwan, 2010, pp. 863–870.

[24] T. Mahl, A. E. Mayer, A. Hildebrandt, and O. Sawodny, "A variable curvature modeling approach for kinematic control of continuum manipulators," in *2013 American Control Conference.*, Washington, DC, 2013, pp. 4945–4950.

[25] D. Trivedi, A. Lofti, and C. Rahn, "Geometrically exact dynamic models for soft robotic manipulators," in *Proc. IEEE/RSJ Int. Conf. Intel. Robot. Syst.*, San Diego, CA, 2007, pp. 1497–1502.

[26] S. Sadati, S. E. Naghibi, A. Shiva, I. D. Walker, K. Althoefer, and T. Nanayakkara, "Mechanics of continuum manipulators, a comparative study of five methods with experiments," in *Towards Autonomous Robotic Systems*, Surrey, UK,, 2017, pp. 686–702.

[27] H. Al-Fahaam, S. Davis, and S. Nefti-Meziani, "A novel, soft, bending actuator for use in power assist and rehabilitation exoskeletons," in *Proc. IEEE/RSJ Int. Conf. Intel. Robot. Syst.*, Vancouver, BC, Canada, 2017, pp. 533–538.

[28] K. Hsiao and H. Mochiyama, "A wire-driven continuum manipulator model without assuming shape curvature constancy," in *Proc. IEEE/RSJ Int. Conf. Intel. Robot. Syst.*, Vancouver, BC, Canada, 2017, pp. 436–443.

[29] M. Giorelli, F. Renda, M. Calisti, A. Arienti, G. Ferri, and C. Laschi, "A two dimensional inverse kinetics model of a cable driven manipulator inspired by the octopus arm," in *Proc. IEEE Int. Conf. Robot. Autom.*, Saint Paul, Minnesota, USA, 2012, pp. 3819–3824.

[30] I. Singh, Y. Amara, A. Melingui, P. Pathak, and R. Merzouki, "Modeling of continuum manipulators using pythagorean hodograph curves," *Soft Robotics*, vol. 5, no. 4, pp. 425–442, Aug. 2018.

[31] I. D. Walker, "Continuous backbone continuum robot manipulators," *ISRN Robotics*, vol. 2013, pp. 54–63, 2013.

[32] B. Jones and I. Walker, "Kinematics of multisection continuum robots," *IEEE Trans. Robot.*, vol. 22, no. 1, pp. 43–57, Feb. 2006.

[33] M. Hannan and I. Walker, "Kinematics and the implementation of an elephant trunk manipulator and other continuum style robots," *J. Robot. Sys.*, vol. 20, no. 2, pp. 45–63, Feb. 2003.

[34] Y. Chen, Y. Cai, J. Zheng, and D. Thalmann, "Accurate and efficient approximation of clothoids using bezier curves for path planning," *IEEE Trans. Robot.*, vol. 33, no. 5, pp. 1242–1247, Oct. 2017.

[35] Levien and Raph, "The euler spiral: a mathematical history," 2008.

[36] F. Daerden and D. Lefebe, "Pneumatic artificial muscles: actuators for robotics and automation," *European journal of mechanical and environmental engineering*, vol. 47, pp. 10–21, 2000.

[37] M. Grissom, V. Chitrakaran, D. Dienno, M. Csencsits, M. Pritts, B. Jones, W. McMahan, D. Dawson, C. Rahn, and I. Walker, "Design and experimental testing of the octarm soft robot manipulator," in *Proc. SPIE Conf. Unmanned Sys. Tech.*, Kissimee, FL, 2006, pp. 109–114.

[38] M. R. Hasan, R. Vepa, H. Shaheed, and H. Huijberts, "Modelling and control of the barrett hand for grasping," in *International Conference on Computer Modelling and Simulation*, Cambridge, UK, 2013, pp. 230–235.

[39] A. Arienti, M. Calisti, F. Giorgio-Serchi, and C. Laschi, "Poseidrone: Design of a soft-bodied rov with crawling, swimming and manipulation ability," in *2013 OCEANS - San Diego*, San Diego, CA, 2013, pp. 1–7.

[40] P. S. Gonthina, "Novel parallel continuum robot grippers and their modeling," Master's thesis, Clemson University, 2018.